**Report No: 24000/13/15**

**Date: 04 September 2015**

**For: Department for Transport**

# Department for Transport Technical Assessment of Petroleum Tankers: Metallographic and Analytical Assessment of AT11-1475

**TWI Ltd**

TWI is one of the world's foremost independent research and technology organisations, with expertise in solving problems in all aspects of manufacturing, fabrication and whole-life integrity management technologies.

Established at Abington, Cambridge, UK in 1946 and with facilities across the globe, the company has a first-class reputation for service through its teams of internationally respected consultants, scientists, engineers and support staff. The company employs over 900 staff, serving over 700 Member companies across 4500 sites in 80 countries.

TWI is a non-profit distributing company, limited by guarantee and owned by its Members. It can therefore offer confidential, independent advice and is internationally renowned for employing multidisciplinary teams to implement established or advanced joining technology or to address issues associated with initial design, materials selection, production and quality assurance, through to service performance and repair.

Supported by a successful international training and examinations network, TWI also takes technical and practical knowhow to regions looking for growth through skills development.

TWI houses the National Structural Integrity Research Centre for postgraduate education, and a professional institution, The Welding Institute, which has a separate membership of over 6000 individuals.

The company operates a management system certificated by LRQA to BS EN ISO 9001:2008. It also has certificated management systems for health and safety (BS OHSAS 18001) and environment (BS EN ISO 14001).

**(See inside back cover TWI Management System.)**

# TWI Report: Department for Transport Technical Assessment of Petroleum Tankers: Metallographic and Analytical Assessment of AT11-1475

## Report No: 24000/13/15

## Date: 04 September 2015

Prepared for: Department for Transport
c/o Zone 2/31
Great Minster House
33 Horseferry Road
London
SW1P 4DR

Contact: Steve Gillingham

Author: Tyler London

## TWI Endorsement

This report has been reviewed in accordance with TWI Policy

Project Leader (Signature) Tyler London

Print name: Tyler London

Technical Reviewer (Signature) pp CM Worrich

Print name: Simon Smith

Approved by (Signature) Ian Norris
Product Manager

Print name: Ian Norris

Approved by (Signature)
Group Commercial Manager

Print name: Andrew Carey

Administrator (Signature) ERaven

Print name: Emma Raven

er

## Published Version History

| Date | Version | Reason |
|---|---|---|
| 29/05/2015 | 0.1 | Draft Issue |
| 10/07/2015 | 0.2 | Draft issue incorporating consortium comments |
| 27/07/2015 | 0.3 | Additional editorial changes |
| 04/09/2015 | 1.0 | Incorporation of consortium comments |

## Contents

# 1 Introduction

As part of the Department for Transport (DfT) research programme on petroleum road fuel tankers, the Health and Safety Laboratory (HSL) has performed a full-scale topple test of the petroleum road fuel tanker AT11-1475. Under Work Package 2 Extensions of the DfT research programme, TWI has been requested to provide numerical analysis and metallographic examinations of sections removed from AT11-1475 after the topple test in order to provide supporting information for the Health and Safety Laboratory (HSL) technical report.

This report details the examination of sections removed from the front and rear ends of the tanker as well as finite element analyses (FEA) that were undertaken to provide insight into the performance of AT11-1475 under the topple test conditions.

# 2 Objectives

The objectives of the present work are to undertake:

- A detailed macroscopic and microscopic examination of sections from the front and rear circumferential joints of tanker AT11-1475.
- Tensile testing on samples machined from the parent metal, weld metal and extrusion band metal.
- FEA in conjunction with a forming limit diagram to determine the likelihood of failures in the parent metal during a topple test.

# 3 Post-mortem and Metallographic Examination

## 3.1 Overview

Petroleum road fuel tanker AT11-1475 is an aluminium-bodied, banded-design. Each adjacent barrel or cylindrical section of aluminium alloy 5182 (henceforth referred to as the 'tanker shell') is joined by a circumferential joint similar to the informative joint design D.14(b) and D.14(c) from BS EN 13094 (2015) shown in Figure 1. In this joint configuration, the partition dish, bulkhead, baffle or end dish is also made of AA 5182. For the rear band (referred to in the main report as band J/10 rear), where there is no adjacent section of tanker shell, only one primary circumferential weld is made. All other circumferential joints except for the front joint are similar to that shown in Figure 1. However, due to the unique design of the front 'swept' dish of AT11-1475 (see, for example, Figure 3), the front-most circumferential joint (referred to in the main report as band A/10 front) is a double-sided corner joint between the dish and the tanker shell, similar to D.9(b) from BS EN 13094 (2015) also shown in Figure 1.

Following the topple test, sections of the undamaged nearside and the impacted offside were removed from AT11-1475 from both the front and rear of the tanker and sent to TWI by HSL. Images of the approximate locations of the sections are shown in Figure 2 for the rear of the tank and in Figure 3 for the front of the tank. Following receipt, the sections were photographed, radiographed, and then additional sampling was undertaken to analyse cross-sections of the circumferential joints.

## 3.2 Radiographic examination

Radiographic inspection was undertaken to identify the location and position of potential welding defects in each of the sections.

For the rear end sections, the primary circumferential welds (ie those joining the tanker shell to the extrusion band) were radiographed. For the rear offside

 

(impacted side) section, the datum markers are shown in Figure 4 and the radiographic interpretation is summarised in Table 1. For the rear nearside section, the datum markers are shown in Figure 5 and the radiographic interpretation is summarised in Table 2.

For the front end sections, the circumferential joint between the swept front dish and the first tanker compartment was radiographed. For the front offside (impacted side) section, the datum markers are shown in Figure 6 and the radiographic interpretation is summarised in Table 3. For the front nearside section, the datum markers are shown in Figure 7 and the radiographic interpretation is summarised in Table 4.

### 3.3 Metallographic examination of samples

Based on the shape of the deformed sections and the results of the radiographic examination, amongst other considerations, the four large sections were sampled at between three and seven different locations each along their circumferential length. Table 5 summarises the sample IDs, the section from which they were machined, and an approximate description of the location of each sample.

Seven samples were machined in the longitudinal direction (transverse to the circumferential welds) from the impacted, rear offside section of AT11-1475. The locations of the samples are shown in Figure 8. From the seven samples, five were removed from the crushed region of the section that impacted the ground during the topple test. The remaining two samples were taken from a region remote from the impact zone: one sample (RO-01) was removed where there was no additional internal fillet weld present (see 'F' in Figure 1), and the other (RO-02) was removed from a location near RO-01 where an additional internal fillet weld was present. For the rear band of AT11-1475, the internal fillet welds were 'stitched' around the circumference, with 50mm weld lengths and 50mm gaps between the welds. In Figure 9, images of samples RO-01, RO-02 and RO-03 are shown. Sample RO-01 and RO-03 exhibit porosity and lack of penetration into the root of the weld, resulting in an approximately 2.0mm deep, surface-breaking, lack of fusion defect. Sample RO-02, however, shows good penetration into the root and there is no lack of fusion defect present. Images of the remaining samples (RO-04 to RO-07) are shown in Figures 10 and 11. In Sample RO-04 (Figure 10), the internal fillet weld joining the toe of the extrusion band to the inner surface of the tanker shell has failed with a crack propagating along the fusion line with the inner surface of the tanker shell. Images of the RO-05, RO-06 and RO-07 from the rear offside are shown in Figure 11. All of these samples exhibit surface-breaking, lack of root fusion defects due to the weld not fully penetrating into the root. The typical depth of these defects ranges from 1.0mm to 2.0mm. For comparison, macro-images of all of the primary circumferential welds (see 'C' in Figure 1) are shown together in Figure 12. In these images, the penetration into the root of the weld is variable. Due to the absence of a through-wall rupture, no additional sampling was undertaken between samples RO-03 and RO-07, and therefore it is not possible to specify the precise circumferential (surface) length of these lack of fusion, surface-breaking defects; however, since the lack of fusion is evident on samples RO-03 through RO-07, in view of the radiography, it is possible to conservatively estimate that the lack of fusion persists continuously between these sampling points and hence has a total surface length of approximately 700mm.

Four samples were machined from the undamaged, rear nearside section of AT11-1475. The locations of the samples are shown in Figure 13. The four

 

samples were spaced approximately 125mm apart. Samples RN-01 to RN- are shown in Figure 14. All of the primary circumferential welds from the rear nearside samples are shown in Figure 15. As with the rear offside, the penetration into the root of the weld is variable, with sample RN-03 exhibiting good penetration and fusion between the tanker shell and extrusion band, whilst samples RN-01, RN-02 and RN-04 show signs of lack of fusion at the root of the weld, resulting in surface-breaking defects that are up to 1.5mm deep.

The main circumferential welds in the samples from both the rear offside and rear nearside were shown to exhibit weld caps (or overfill) typically in excess of 3.0mm as measured from the outer surface of the tanker shell. Previous research on tanker performance under topple test conditions (TWI, 2015) has demonstrated the benefits that a large weld cap can have in resisting the bending moments experienced by the joint under topple test conditions. Nevertheless, an excessive weld cap can also be indicative of poor root penetration, which is evident in many of the samples taken from the rear welds. All weld samples from the rear offside and rear near side showed very good alignment, with axial misalignment measurements typically being less than 0.5mm. The previous TWI research (2015) also demonstrated the significant effect of misalignment on the acceptability of defects; specifically, the maximum tolerable defect size under topple test conditions reduced rapidly as the level of axial misalignment increased. Thus, although a surface-breaking, lack of root fusion defect is present in many of the rear weld samples, it is likely that the combination of good joint alignment and relatively large weld cap size contributed to the lack of failure during the topple test.

Six samples were machined in the longitudinal direction from the impacted, front offside section of AT11-1475. As described in Section 3.1, all circumferential joints in AT11-1475 are geometrically similar to that shown in Figure 1 except for the front-most joint, which is a double-sided corner joint due to the swept design of the front dish. Of the six samples, five were taken from the crush zone (ie the large plastic bulge that comprises the flattened region that impacted the ground) and one additional sample (FO-01) was taken remote from the crush zone. The locations of the samples are illustrated in Figure 16. In Figure 17, images of the corner joint are shown for each sample from the front offside. Whilst the front circumferential joint has undergone extensive plastic deformation during the topple test as evidenced by the severe bending shown in Figure 17, none of these exhibit any evidence of cracking.

Finally, three samples were machined from the undamaged, front nearside of the tank as illustrated in Figure 18. Images of the welds from these samples are shown in Figure 19.

## 3.4 Tensile testing

Tensile testing was undertaken on material samples machined from the undamaged rear, nearside section of AT11-1475.

Two tensile specimens were prepared from the tanker shell material in the joints shown in Figure 20 (labelled M01-01 and M01-02). These specimens were taken in the circumferential orientation and machined as flat bar specimens. Weld metal specimens could not be machined from the primary circumferential welds joining the tanker shell to the extrusion band because of the need to avoid the potential presence of lack of fusion defects that could affect the tensile testing results. Instead, two flat bar, all-weld metal specimens were machined from the weld joining the rear dish to the top of the extrusion band (see the top weld labelled ‘E’ in Figure 1). These specimens are labelled M02-01

 

and M02-02 in Figure 20. Finally, two round bar specimens were machined from circumferentially-oriented material from the centre of the up-stand of the extrusion band. These specimens are labelled M03-01 and M03-02 in Figure 20.

The flat bar tensile specimens were of nominal width 6.0mm and parallel length 32.0mm, marked with a 25.0mm gauge length for determination of plastic elongation. The specimens were instrumented with a dual averaging HRD auto extensometer of gauge length 25.0mm for the determination of total elongation (at fracture) and tested at ambient temperature. The choice of ambient temperature instead of the minimum ADR design temperature (-20°C) was made to more closely match the conditions of the topple test. The applied strain was recorded through the entire test. Up to the yield point, the applied strain rate was 0.015 strain/min, and beyond the yield point, the applied strain rate was 0.400 strain/min.

The round bar tensile specimens were of nominal diameter 8.0mm and parallel length 48.0mm, marked with a 5X diameter gauge length for determination of plastic elongation. The specimens were instrumented with a dual averaging extensometer and tested at ambient temperature.

The stress-strain curves showed that the weld metal slightly overmatches the tanker shell metal, and that the tanker shell metal has tensile properties that are generally in agreement with the anticipated properties of the aluminium alloy Al-5182. The extrusion band metal significantly overmatches both the parent and weld metal curves, exhibiting a higher yield point, ultimate tensile strength and smaller elongation.

# 4 Forming Limit Diagram Assessment

## 4.1 Overview

In order to provide additional numerical and analytical understanding of the performance of the tanker under the topple test conditions, finite element analyses have been conducted on the front and rear circumferential joints. The FEA performed and described in this report is a simplified, static model of the topple test. The dynamic and inertial effects experienced during the actual topple test are ignored and only the deformation of the tank due to the 'crushing' effect of the ground and the pressure exerted by the water contained in the compartments on the internal surfaces of the tank are considered. The results of the FEA have been assessed using a forming limit diagram methodology to determine whether ruptures in the parent metal or weld metal would occur due to the deformation exceeding the formability limit of the tanker shell material, Al-5182.

## 4.2 Finite element modelling

### 4.2.1 Software

All models were generated using version 6.14-1 of the pre-processing finite element analysis software Abaqus/CAE and the analyses were solved using version 6.14-1 of Abaqus/Standard (SIMULIA, 2014).

### 4.2.2 Geometry

Two different models were created: one for the rear dish and one for the front dish. All models were created using the CAD capabilities of Abaqus/CAE and were developed from engineering drawings provided by Lakeland Ltd (2004a-c, 2005, 2011, 2015). The dimensions in the engineering drawings were compared with those measured from the sections of AT11-1475 received from HSL and

 

any differences were incorporated into the model as appropriate. Due to symmetry considerations with respect to the geometry and applied loads, only one-quarter of the rear and front sections were modelled.

The rear dish model comprised of the extrusion profile, rear dish and tanker shell. In order to facilitate the accurate resolution of the extensive bending that the rear dish undergoes during the topple test, the rear dish was modelled as a shell part and meshed with quadratic, reduced-integration, shell elements (type S8R in Abaqus) with nine integration points through thickness. The rest of the geometry was modelled as a solid body. Except for the regions that were in contact with the ground, all solid regions were meshed with 20-node, quadratic-displacement, reduced-integration elements (type C3D20R in Abaqus). In order to improve contact convergence, several layers of elements that would be in contact with the ground were meshed with 8-node, linear-displacement, reduced-integration elements (type C3D8R in Abaqus). A tie constraint was used to join the incompatible interfaces between the solid linear elements and solid quadratic elements. A shell-to-solid coupling was defined between the shell part (rear dish) and the solid part (extrusion band) to ensure continuity of displacements and rotations across this interface. Images of the geometry, finite element mesh and boundary conditions for the rear dish are shown in Figure 21 and 22.

The front dish model was modelled as a single, solid body and comprised entirely of solid, quadratic continuum elements. Images of the geometry, finite element mesh, and boundary conditions for the front dish are shown in Figure 23 and 24.

### 4.2.3 Material properties

Two different material regions were included in the rear dish model: one for the tanker shell, weld metal and rear dish, and one for the extrusion band. For both regions, the lower-bound engineering stress-strain curves obtained from tensile testing were transformed to true stress-true plastic strain curves and sampled at 20-30 equally-spaced points. For both materials, the Young's modulus was taken to be 70GPa and the Poisson's ratio was taken to be 0.3, which agree with the test measurements and with the typical elastic constants for this material (MatWeb, 2015). A rate-independent plasticity model using the Von Mises yield criterion and isotropic strain hardening rule was specified using the incremental plasticity data obtained from sampling the tensile curves. In the front dish model, no extrusion band was present, and the entire model was comprised of the lower-bound parent metal material.

### 4.2.4 Loads and boundary conditions

A flat, analytic rigid body was created to model the ground and was coupled to a centrally-positioned reference node. All degrees of freedom of this reference node were restrained (set equal to zero) except for U2, the translational degree of freedom in the crushing direction. A contact definition was created between the ground and the tanker model with hard, normal contact and a penalty friction coefficient of 0.1. A 250mm displacement was applied in the crushing direction (ie into the tanker section) to simulate the static impact of the ground and tank. The magnitude of this displacement is somewhat arbitrary, as it was chosen to be sufficiently large so as to ensure the simulation would achieve the same flattened length measured from the specimens after the topple test (see Section 4.2.5). The boundary conditions applied to the tanker geometry were those representing the symmetry planes and axial restraint, simulating the longer adjacent section of tanker that was not incorporated into the model. All

 

simulations were analysed with the finite strain formulation, incorporating the nonlinear effects of large displacements and rotations.

### 4.2.5 Results

After the topple test, the flattened length of the rear band (ie the length of the crush zone) was approximately 760mm, and the flattened length of the front circumferential joint was approximately 580mm. Therefore, for each simulation, the ground was translated into the tanker model until the flattened length of the deformed model matched that measured on the sections removed from AT11-1475.

The deformation and Von Mises stress contour for the rear dish model is shown in Figure 25 at the solution increment when the flattened length was 760mm. The deformation of the rear dish model showed exceptional agreement with the samples taken from the rear, offside section of AT11-1475. In particular, the shape, curvature and dimensions of the crush zone agreed with the samples taken from the centre (sample RO-05, see Figure 26) as well as the ends of the crush zone (sample RO-03, see Figure 27). For this reason, the model was considered to be a reasonably accurate representation of the topple test.

The deformation and Von Mises stress contour for the front dish model is shown in Figure 28 at the solution increment when the flattened length was approximately 580mm. As with the rear band model, the front dish model showed very good agreement with measurements taken from samples of the front, offside section of AT11-1475.

To assess the likelihood of cracking occurring in the parent or weld metal, a forming limit diagram (FLD) approach was employed. Technical details about the forming limit diagram methodology are provided in Li (2011), Abedrabbo et al (2006) and Soare (2007). Essentially, a forming limit diagram provides a graphical description of material failure tests such as biaxial tension tests and punched dome tests. The diagram comprises a 'safe' region and an 'unsafe' region separated by the forming limit curve. The forming limit curve is defined as a locus of points with x-coordinate minor strain and y-coordinate major strain. FLDs are typically employed in the sheet metal forming industry to determine the propensity for cracks to appear during cold-forming, bending and stamping. Due to the thin nature of sheets, the through-wall strains are negligible, and therefore the strain state at any given point can be wholly described by the minor and major principal strains. For the present analyses, the large span of the end dishes relative to the wall thickness enables the forming limit diagram approach to be used. A literature review of FLDs for Al 5182-O, the aluminium alloy of the end dishes and tanker shell, was undertaken to provide an approximate forming limit curve suitable for the present analysis. Whilst FLDs have some dependency on strain-rate, thickness, temperature, heat treatment and pre-strain, a representative curve, obtained from the literature review (Wu et al, 2003), was employed for the present study. The results obtained from this forming limit curve described below have provided reasonable comparisons to the topple test results, and therefore these additional dependencies had only secondary influences.

For the rear band model, a circumferential path of nodes was created in the region where the principal strains were largest. This path of nodes was located on the inner surface of the rear dish at the extrados (tensile side) of the bend comprising the crushed zone. For each node in this path, the maximum principal (major) strain and minimum principal (minor) strain were output at the solution increment when the flattened length was 760mm. The pairs of

 

minor strain and major strain were plotted on the FLD against the forming limit curve from Wu et al (2003) as shown in Figure 29. In this figure, the red curve (strains from the FE model) lies below the forming limit curve (black curve). This indicates that the forming limit diagram approach does not predict failure to occur. This result agrees with the observations from the topple test and subsequent metallographic examinations, where no cracking or failure of the rear dish was seen.

For the front dish model, a circumferential path of nodes was created along the corner joint between the swept design front dish and the tanker shell. As with the rear band model, the maximum and minimum principal strains were extracted at each node on this path and the results were plotted on the forming limit diagram in Figure 30. Again, the strains from the model all lie below the forming limit curve and hence the FLD approach does not predict failure to occur, which agrees with the lack of failure observed in the front dish after the topple test and subsequent metallographic examinations.

# 5 Conclusions

Metallographic examinations and detailed numerical analyses have been undertaken to provide supplementary information about the performance of the petroleum road fuel tanker AT11-1475 after topple testing. These investigations found that:

1. No through wall ruptures were observed in any of the samples taken from the front or rear welds of AT11-1475.
2. The samples from the front circumferential joint did not exhibit any significant lack of fusion defects.
3. The samples of the rear circumferential joint exhibited variable root penetration in the main circumferential welds. This resulted in some internal surface-breaking, lack of root fusion defects being observed with typical defect depths ranging from 1.0mm to 2.0mm.
4. For the rear weld samples, the joints were found to exhibit good alignment, typically within 0.5mm, and the height of the weld caps of the main circumferential welds was found to be typically in excess of 3.0mm. The combination of low misalignment and large weld caps likely contributed to the good performance of the joints under the topple test. However, the excessive weld cap size was seen to correlate with lack of root penetration (and lack of root fusion defects) in many samples.
5. Finite element modelling of a static, idealised representation of the end dish under topple test conditions in conjunction with a forming limit diagram methodology correctly predicted that the front swept dish and rear end dish of AT11-1475 would not rupture during the topple test. The model also accurately predicted the tanker front swept dish and rear end dish deformations and therefore represents a valuable approach for future assessments of tanker performance under these conditions.

# 6 References

Abedrabbo N, Pourbogrhat F and Carsley J (2006): 'Forming of AA5182-O and AA5754-O at elevated temperatures using coupled thermo-mechanical finite element models', International Journal of Plasticity, Vol 23, pp 841-875.

BSI (2015): 'BS EN 13094:2015 Tanks for the transport of dangerous goods – Metallic tanks with a working pressure not exceeding 0.5bar – Design and Construction', BSI Standards Publication.

 

Li J (2011): 'Characterization of post-annealing mechanical behaviour of preformed aluminium alloy 5182-O', University of Michigan PhD Dissertation.

Lakeland (2004a): 'Main Division – Semi-trailer', Document Ref: DRG.NO.C2076.

Lakeland (2004b): 'Division – Semi-trailer', Document Ref: DRG.NO.C2082.

Lakeland (2004c): 'Joint Ring 2', Engineering drawing of extrusion profile design, Document Ref: 77605.

Lakeland (2005): 'Large Division / Baffle Extrusion', Document Ref: DRG.NO.C2939.

Lakeland (2011): 'G.A. – 42800L-6C AL.-ADR-BLVF', Document Ref: DRG.NO.B1404.

Lakeland (2015): 'AT11.1475 Test Tank – Front End 1'. Engineering drawing of AT11-1475 tank front end.

MatWeb (2015): 'MatWeb.com: Material Property Data', http://www.matweb.com/search/datasheettext.aspx?matid=9217, accessed 24/07/2015 at 13.54.00.

SIMULIA (2015): 'Abaqus Analysis User's Guide', SIMULIA.

Soare SC (2007): 'On the use of homogeneous polynomials to develop anisotropic yield functions with applications to sheet forming', University of Florida PhD Dissertation.

TWI (2015): 'Department for Transport Technical Assessment of Petroleum Tankers: Work Package 2 – Detailed Engineering Critical Assessment', TWI Report 24000/9/15, 31 March 2015.

Wu PD, Jain M, Savoie J, MacEwen SR, Tugcu P and Neale KW (2003): 'Evaluation of anisotropic yield functions for aluminium sheets', International Journal of Plasticity, Vol 19.

 

**Table 1** Rear offside (impacted side) primary circumferential weld radiographic interpretation for AT11-1475 (see Figure 4)

| Radiograph Number | Weld Number | Datum Points | Comments |
|---|---|---|---|
| P0117 | W1 | A-B | Groove Noted, minor isolated pores throughout <0.8mm ø. |
| P0118 | W1 | B-C | Groove Noted, linear aligned pores throughout <1.0mm ø. |
| P0119 | W1 | C-D | Groove Noted, linear aligned pores throughout <1.0mm ø. |
| P0120 | W1 | D-E | Groove Noted, linear aligned pores throughout <1.0mm ø. |
| P0121 | W1 | E-F | Groove Noted, linear aligned pores throughout <1.0mm ø. |
| P0122 | W1 | F-G | Groove Noted, linear aligned pores throughout <1.0mm ø. |
| P0123 | W1 | G-H | Groove Noted, linear aligned pores throughout <1.0mm ø. |

**Table 2** Rear nearside primary circumferential weld radiographic interpretation for AT11-1475 (see Figure 5)

| Radiograph Number | Weld Number | Datum Points | Comments |
|---|---|---|---|
| P0112 | W3 | A-B | Groove Noted, linear aligned pores throughout <1.0mm ø. |
| P0113 | W3 | B-C | Groove Noted, linear aligned pores throughout <1.0mm ø. |
| P0114 | W3 | C-D | Groove Noted, linear aligned pores throughout <1.0mm ø. |
| P0115 | W3 | D-E | Groove Noted, linear aligned pores throughout <1.0mm ø. |

**Table 3** Front offside weld radiographic interpretation for AT11-1475 (see Figure 6)

| Radiograph Number | Weld Number | Datum Points | Comments |
|---|---|---|---|
| P0151 | W1 | A-B | Linear lack of penetration noted throughout radiograph. Isolated porosity noted no greater than 1mm ø. |
| P0152 | W1 | B-C | Linear lack of penetration noted throughout radiograph. Isolated porosity noted no greater than 1mm ø. |
| P0153 | W1 | C-D | Linear lack of penetration noted throughout radiograph. Isolated porosity noted no greater than 1mm ø. |
| P0154 | W1 | D-E | Linear lack of penetration noted throughout radiograph. Isolated porosity noted no greater than 1mm ø. |
| P0155 | W1 | E-F | Isolated porosity noted no greater than 1mm ø throughout. |
| P0156 | W1 | F-G | Linear porosity noted, F + 10mm for a length of 25mm. Isolated porosity noted no greater than 1.5mm ø throughout. |
| P0157 | W1 | G-H | Porosity noted no greater than 1.5mm ø throughout. |
| P0158 | W1 | H-I | Porosity noted no greater than 1.5mm ø throughout. |
| P0159 | W1 | I-J | Porosity noted no greater than 1.5mm ø throughout. Lack of penetration 20mm up to J. |
| P0160 | W1 | J-K | Porosity noted no greater than 1.0mm ø throughout, transverse void noted positioned J+15mm,4mm long |
| P0161 | W1 | K-L | Porosity noted no greater than 1.0mm ø throughout. Two large pores noted 25mm before L. |
| P0162 | W1 | L-M | Porosity noted no greater than 1.0mm ø throughout. Two gas pores noted, position L +10mm, and L +18mm. Lack of penetration starting 60mm from L to M. |
| P0163 | W1 | M-N | Minor porosity noted throughout. Intermittent Lack of Penetration, position M +20mm. |
| P0164 | W1 | N-O | Minor porosity noted throughout. Intermittent Lack of Penetration, position N +25mm to O. |
| P0165 | W1 | O-P | Minor porosity noted throughout. Linear Pore noted, 4mm ø. |
| P0166 | W1 | P-Q | Minor porosity noted no greater than 0.2mm ø throughout. Lack of penetration throughout. |
| P0167 | W1 | Q-R | Minor porosity noted no greater than 0.5mm ø throughout. 1 gas pore noted, position Q +35mm. Intermittent lack of penetration throughout. |
| P0168 | W1 | R-S | Minor porosity noted no greater than 0.5mm ø throughout. Intermittent lack of penetration throughout. |
| P0169 | W1 | S-T | Minor porosity noted no greater than 0.7mm ø throughout. Intermittent lack of penetration throughout. |
| P0170 | W1 | T-U | Minor porosity noted no greater than 0.5mm ø throughout. Intermittent lack of penetration throughout. |
| P0171 | W1 | U-V | Intermittent lack of penetration throughout. |
| P0172 | W1 | V-W | Intermittent lack of penetration throughout. |
| P0173 | W1 | W-X | 4 gas pores noted, 4mm ø. Minor porosity noted no greater than 0.5mm ø throughout. Intermittent lack of penetration noted at X position. |

**Table 4** Front nearside weld radiographic interpretation for AT11-1475 (see Figure 7)

| Radiograph Number | Weld Number | Datum Points | Comments |
|---|---|---|---|
| P0096 | W1 | A-B | Porosity noted throughout radiograph between 0.2 to 1.3mm ø. Linear lack of fusion noted 60mm from A to 30mm behind B. |
| P0097 | W1 | B-C | Isolated porosity noted throughout radiograph <1.0mm ø. Linear lack of fusion noted 20mm long, 50mm behind C. |
| P0098 | W1 | C-D | Isolated scattered porosity noted throughout radiograph <0.5mm ø. 2 large pores noted at the stop/start no greater than 1.5mm ø. |
| P0099 | W1 | D-E | Isolated porosity noted throughout radiograph <0.5mm ø. Intermittent lack of fusion noted. |
| P0100 | W1 | E-F | Isolated porosity noted throughout radiograph <0.5mm ø. Intermittent lack of fusion noted. |

**Table 5** Summary of cross-section samples for the metallographic examination of AT11-1475

| Section | Sample ID | Description |
|---|---|---|
| Rear offside Figure 8 | AT1-1475-RO-01 | Remote from impact site where there is no internal fillet weld |
| | AT1-1475-RO-02 | Remote from impact side site where this is an internal fillet weld |
| | AT1-1475-RO-03 | End of the crush zone towards the top of the tank |
| | AT1-1475-RO-04 | Located between RO-03 and RO-05 in crush zone |
| | AT1-1475-RO-05 | Centre of the crush zone/bulge |
| | AT1-1475-RO-06 | Located between RO-05 and RO-07 in crush zone |
| | AT1-1475-RO-07 | End of the crush zone towards the bottom of the tank |
| Rear nearside Figure 13 | AT1-1475-RN-01 | Centrally-located, no internal fillet weld |
| | AT1-1475-RN-02 | Centrally-located, internal fillet weld present |
| | AT1-1475-RN-03 | Centrally-located, no internal fillet weld |
| | AT1-1475-RN-04 | Centrally-located, internal fillet weld present |
| Front offside Figure 16 | AT1-1475-FO-01 | Remote from the impact site towards top of tank |
| | AT1-1475-FO-02 | End of the crush zone towards the top of the tank |
| | AT1-1475-FO-03 | Located between FO-02 and FO-04 |
| | AT1-1475-FO-04 | Centre of the crush zone |
| | AT1-1475-FO-05 | Located between FO-04 and FO-06 |
| | AT1-1475-FO-06 | End of the crush zone towards the bottom of the tank |
| Front nearside Figure 18 | AT1-1475-FN-01 | Centrally-located |
| | AT1-1475-FN-02 | Centrally-located |
| | AT1-1475-FN-03 | Centrally-located |

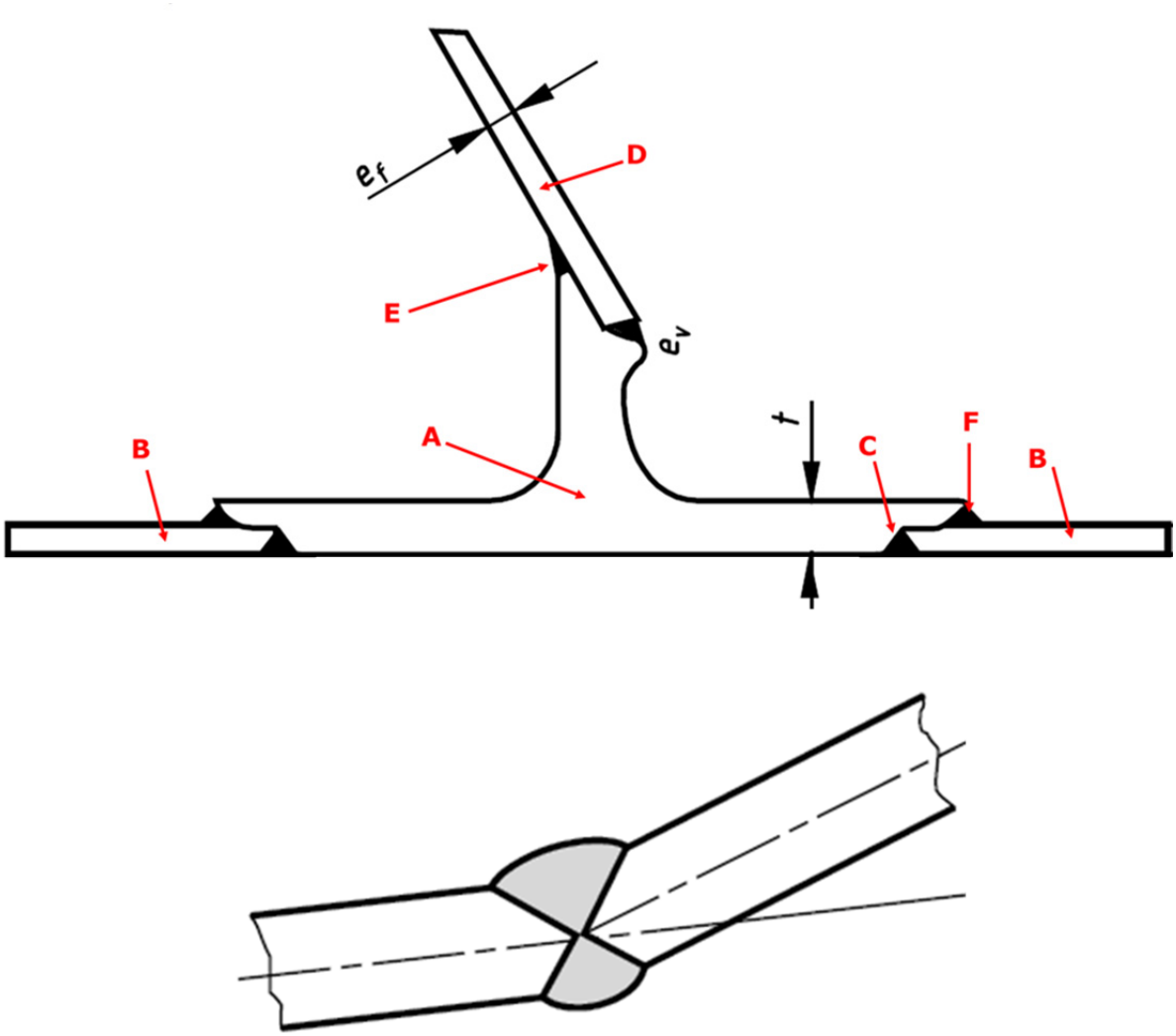


**Figure 1** Diagrams of a joint designs that are qualitatively similar to the rear and intermediate circumferential, extrusion band joints (top frame) and front end joint (bottom frame) in tanker AT11-1475. Images reproduced from Figure D.14(c) for the top frame and D.9(b) for the bottom frame in BS EN 13094 (2015) with red arrows added for this report.

A) Extrusion band (or extrusion profile);
B) Tanker shell;
C) Primary circumferential weld joining tanker shell to the extrusion band;
D) Division plate such as a bulkhead, baffle, surge plate or end dish;
E) 'Top' weld joining the division plate to the extrusion band;
F) Internal fillet weld joining the inner surface of the tanker shell to the extrusion band.


**Figure 2** Locations of the sections removed from the impacted, rear offside of AT11-1475 (Position B) and the undamaged, rear nearside (Position A). Images provided courtesy of HSL.


**Figure 3** Location of the section removed from the impacted, front offside of AT11-1475. Images courtesy of HSL. The position A indicates the approximate dimensions of the section received by TWI.


**Figure 4** Image of the section from the rear offside of AT11-1475 showing the datum markers (A-H for the primary circumferential weld) for the radiographic examination (see Table 1).

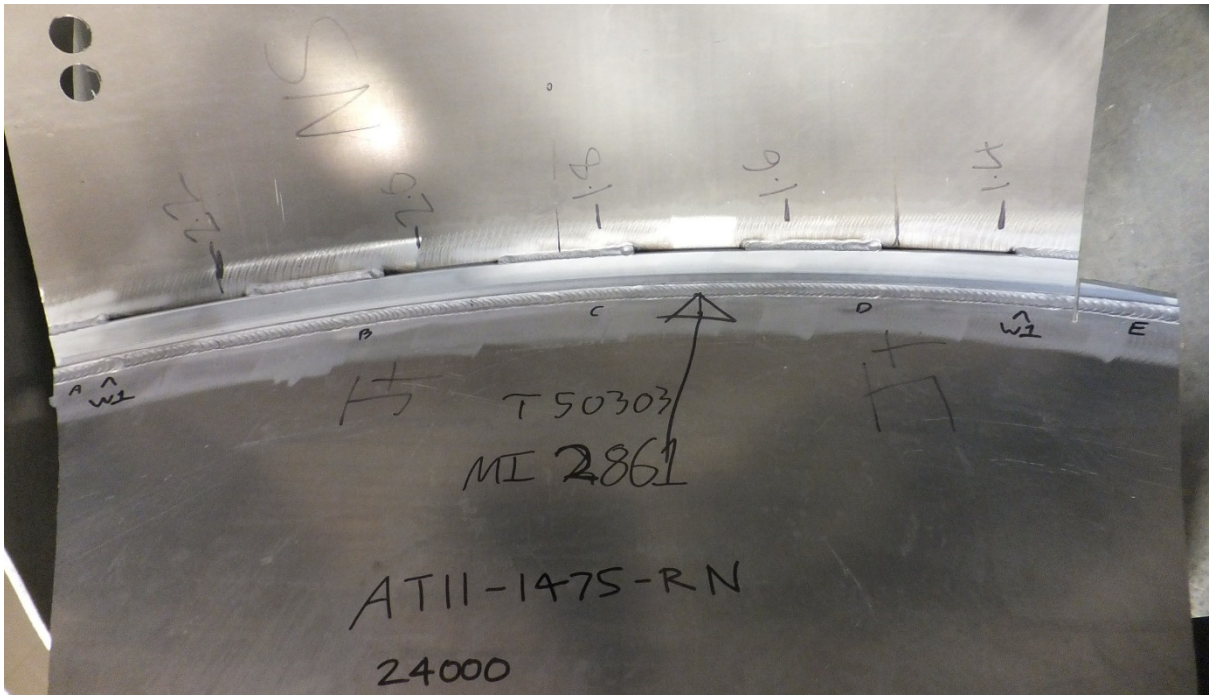


**Figure 5** Image of the section from the rear nearside of AT11-1475 showing the datum markers (A-E) for the radiography (Table 2).

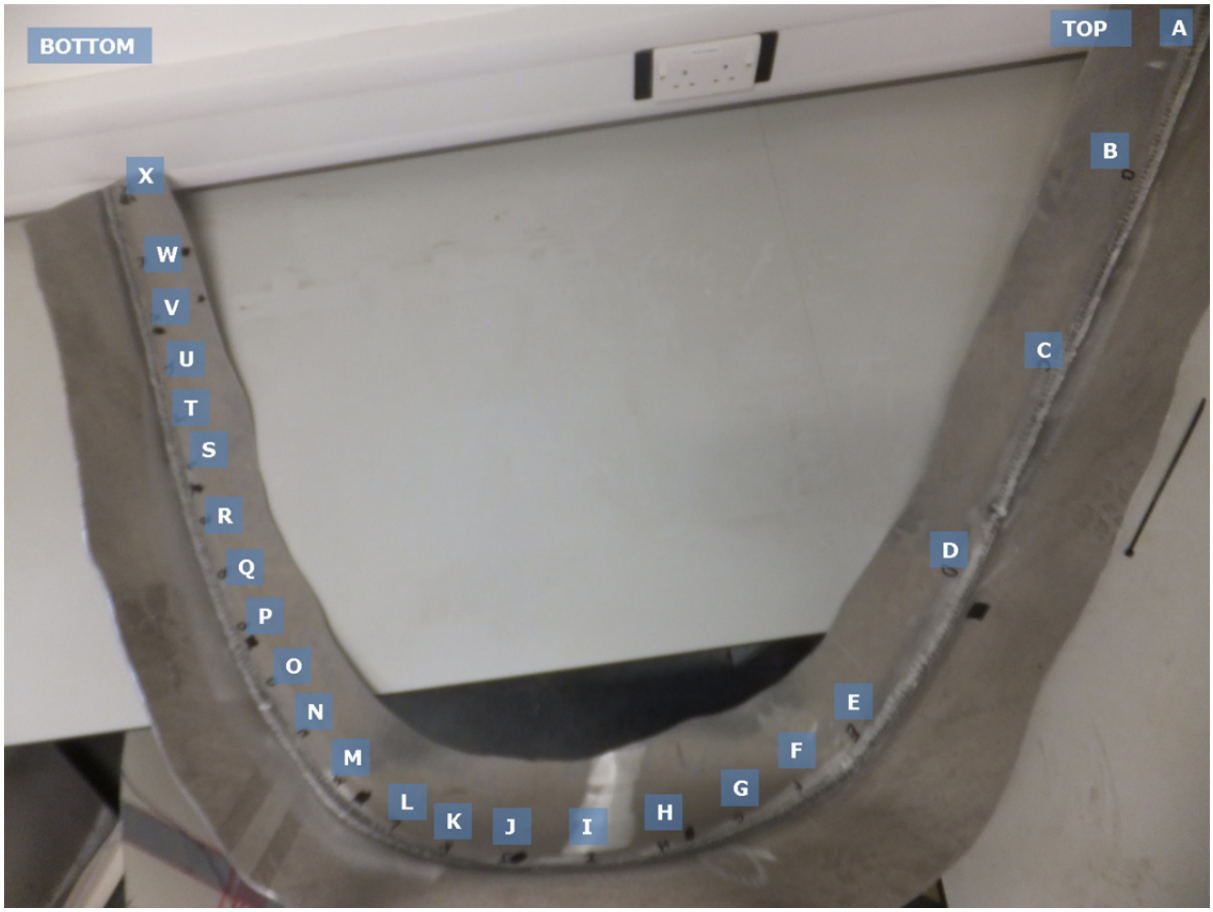


**Figure 6** Image of the section from the front offside of AT11-1475 showing the datum marks (A-X) for the radiography (Table 3).

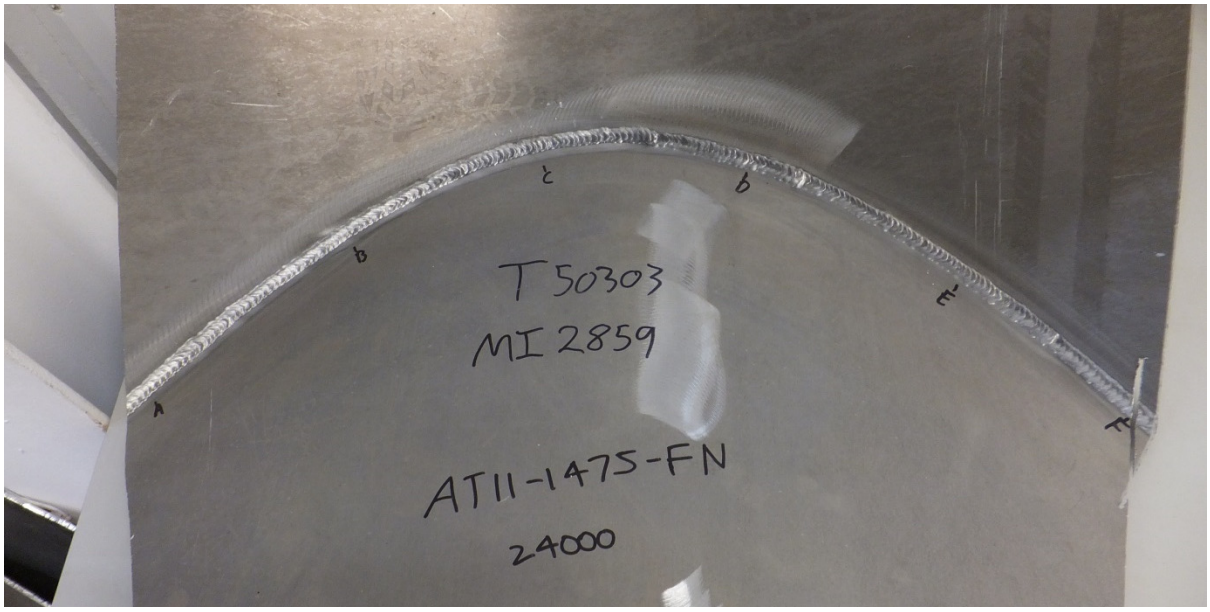


**Figure 7** Image of the section from the front nearside of AT11-1475 showing the datum markers (A-F) for the radiography (Table 4).

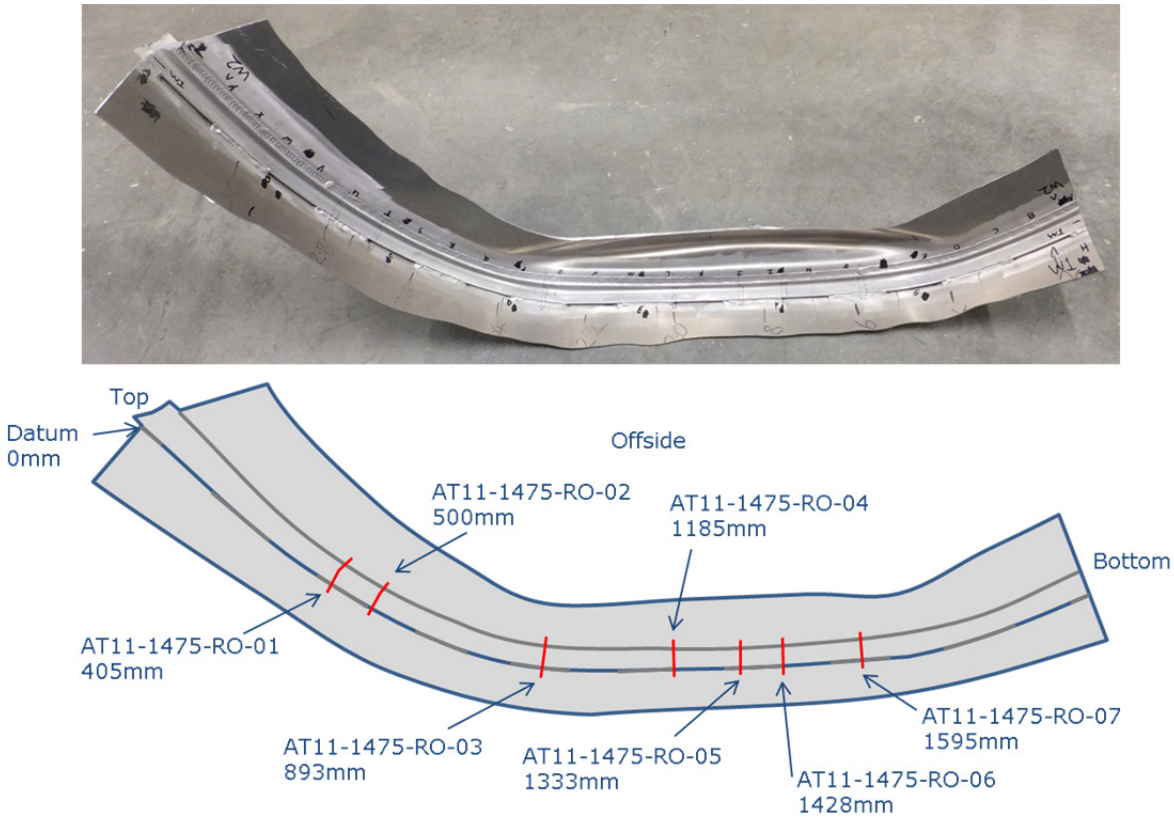


**Figure 8** Diagram of the sampling plan for the rear offside (impacted) section of AT11-1475.

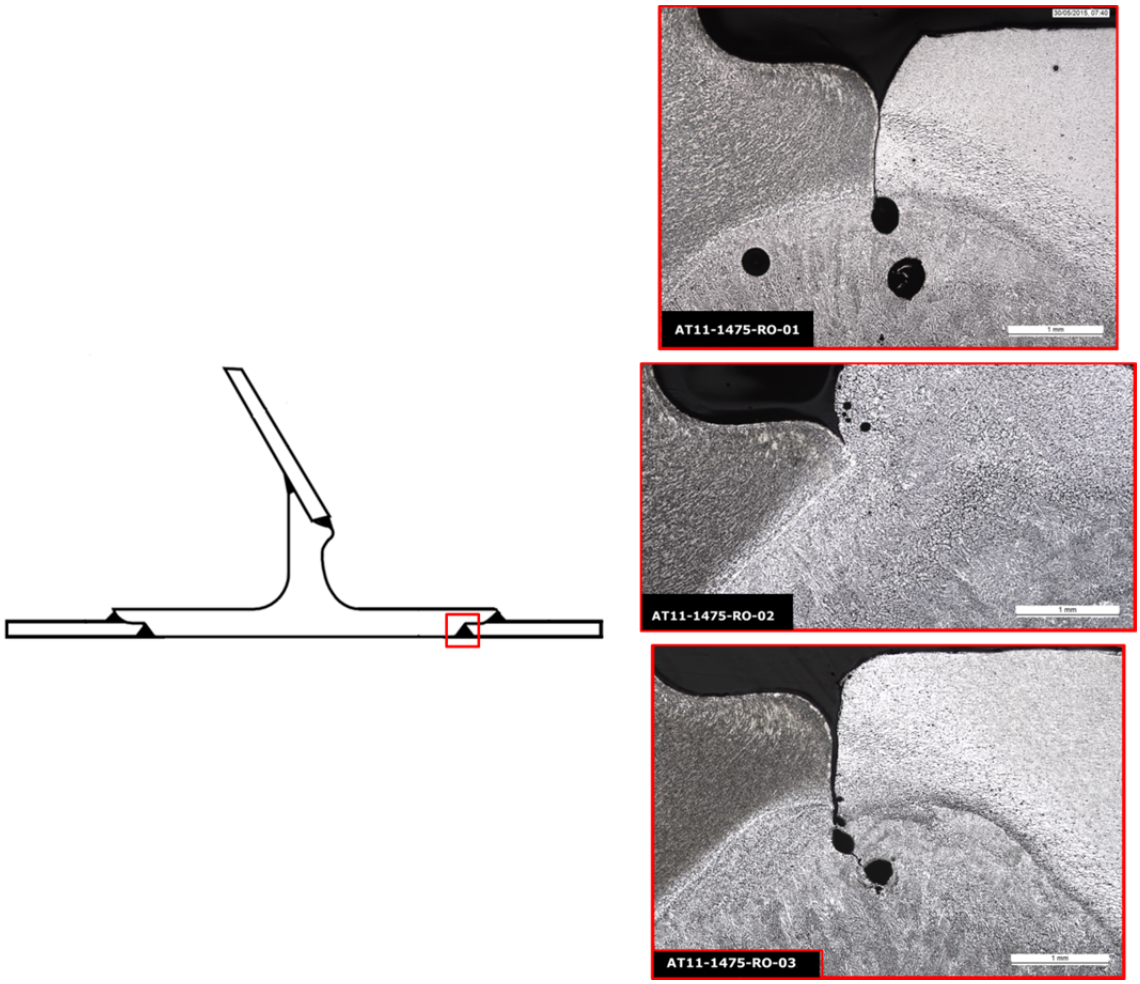


**Figure 9** Images of samples RO-01 (top right), RO-02 (middle right), and RO-O3 (bottom right) with the reference location shown on the BS EN 13094 indicative joint design D.14(c) on the left. The scale bars on the right indicate 1.0mm. Samples RO-01 and RO-03 exhibit lack of root fusion defects, whilst RO-02 exhibits good penetration and fusion.

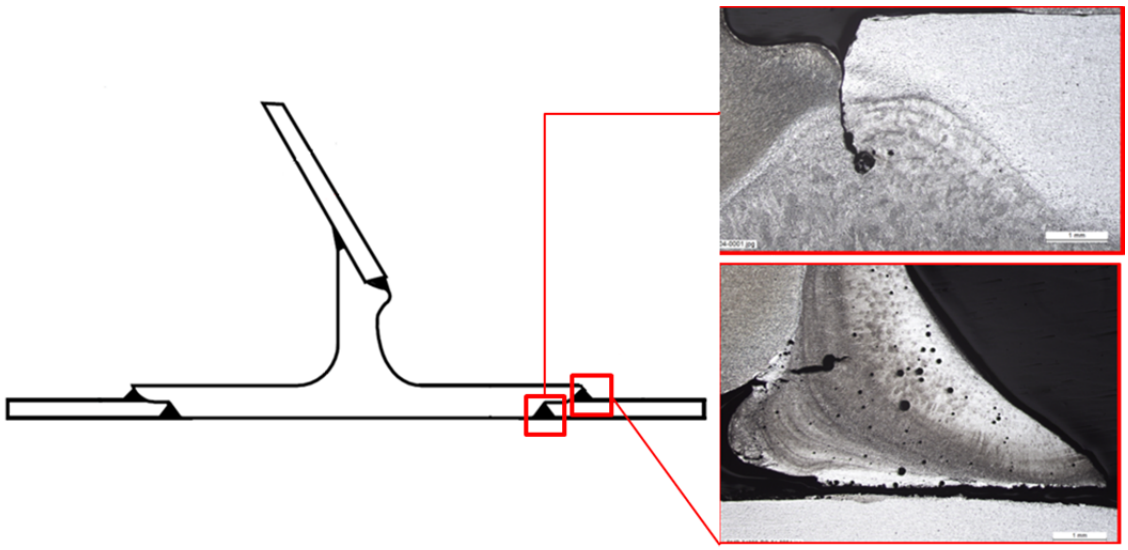

**Figure 10** Images of sample RO-04. On the right images, the scale bars indicate 1.0mm length. The top right image shows the lack of root fusion defect, and the right frame shows the fracture between the internal fillet weld and the inner surface of the tanker shell along the fusion line.

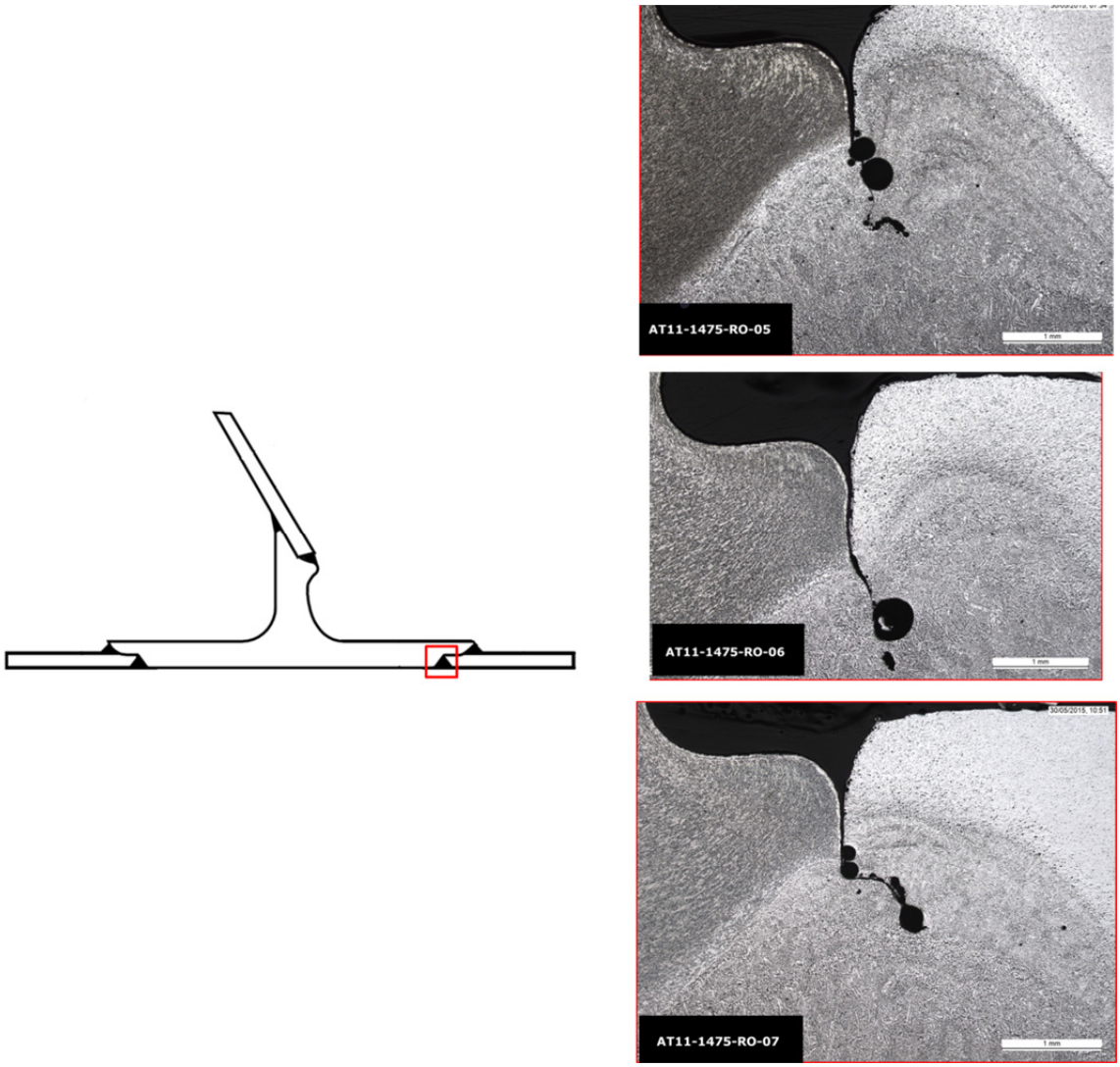


**Figure 11** Images of samples RO-05 (top right), RO-06 (middle right), and RO-07 (bottom right), with the reference location shown on the BS EN 13094 indicative joint design D.14(c) on the left. On the left frames, the scale bar indicates 1.0mm length. All three samples exhibit lack of root fusion defects.

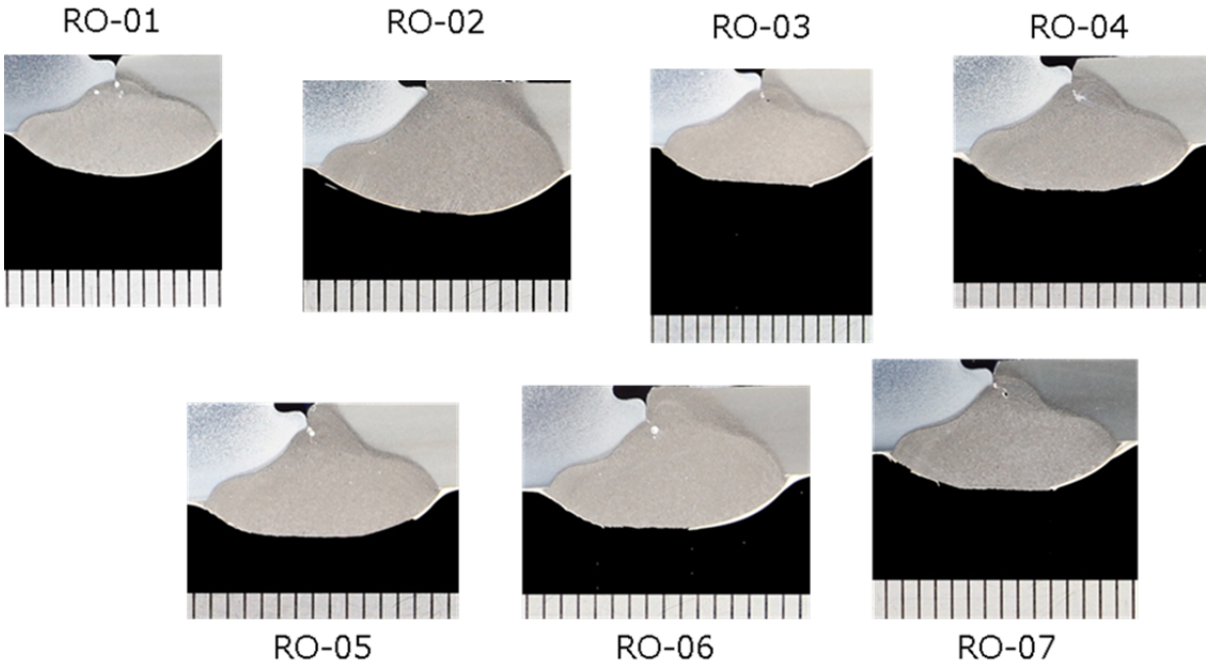


**Figure 12** Images of the circumferential welds from the rear offside section of AT11-1475. Tick marks indicate 1.0mm length. The locations are shown in Figure 8.

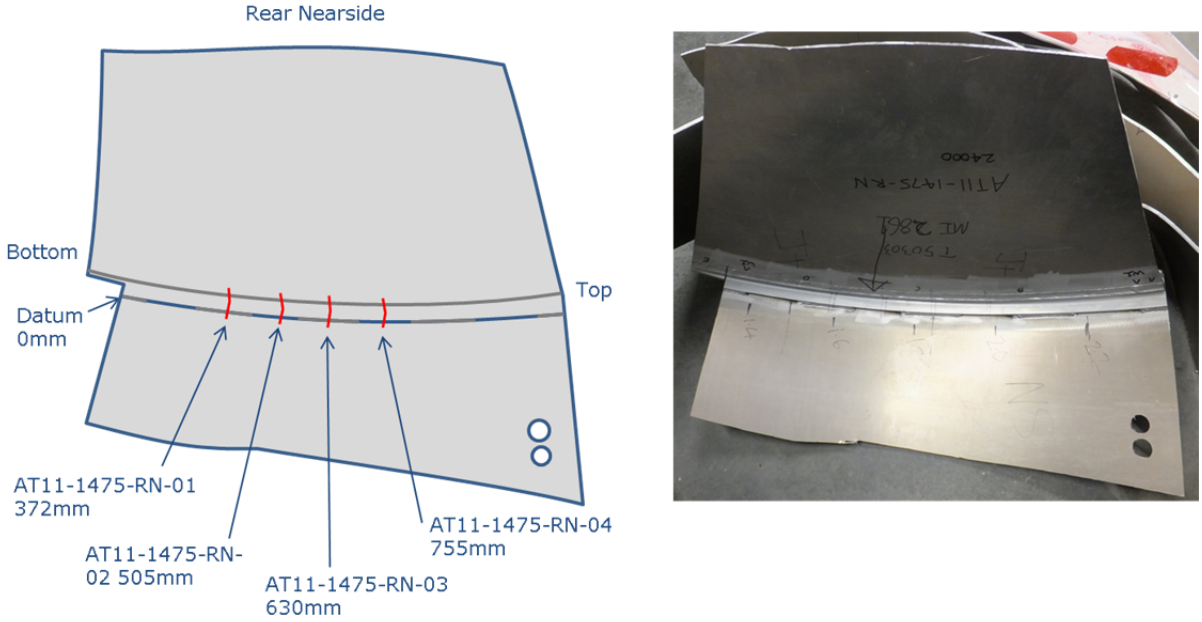


**Figure 13** Diagram of the sampling plan for the rear nearside (undamaged) section of AT11-1475.

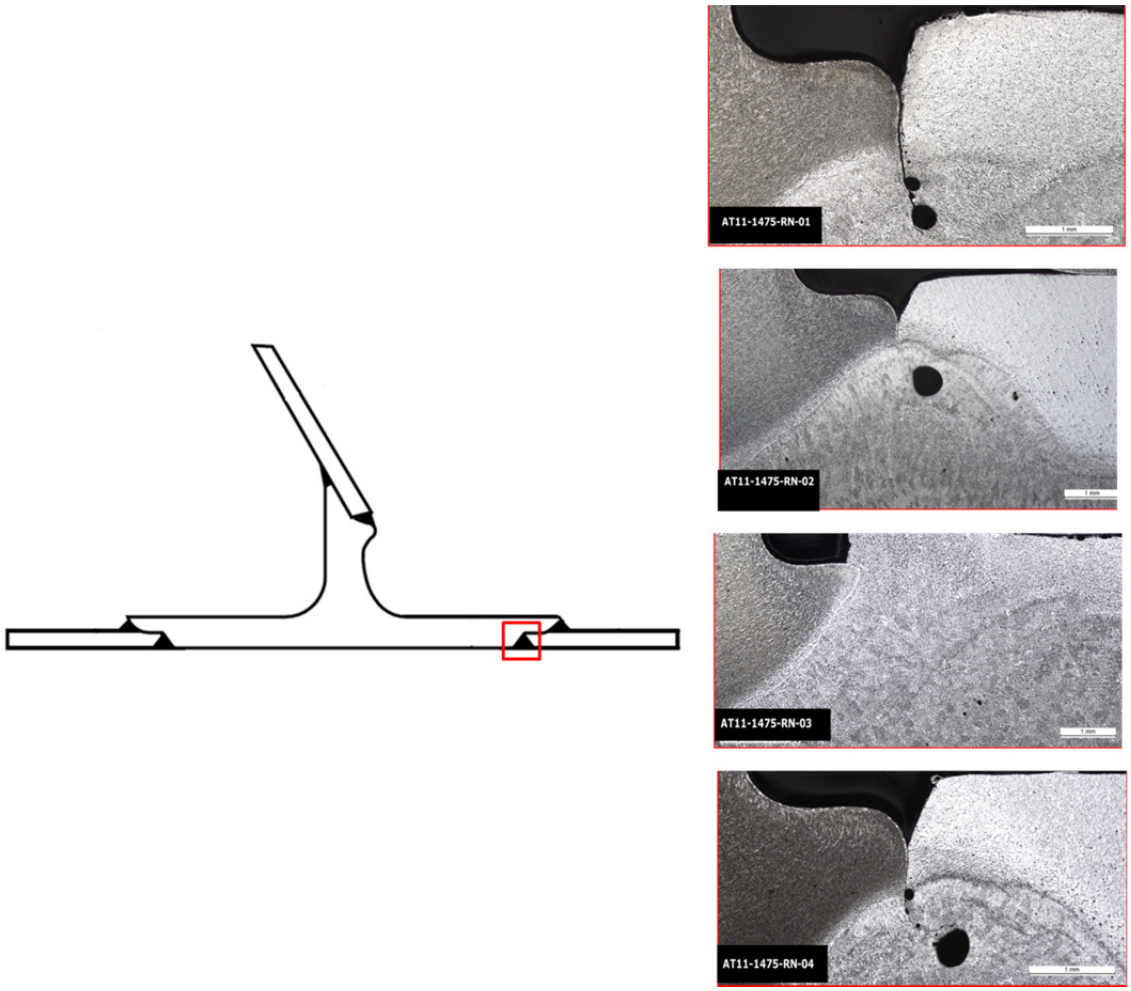


**Figure 14** Images of samples RN-01 (top right), RN-02 (second from top right), RN-03 (third from top right), and RN-04 (bottom right). The scale bars on the frames indicate 1.0mm length. Sample RN-01 shows more significant lack of fusion at the root than RN-02. Sample RN-04 exhibits lack of root fusion.

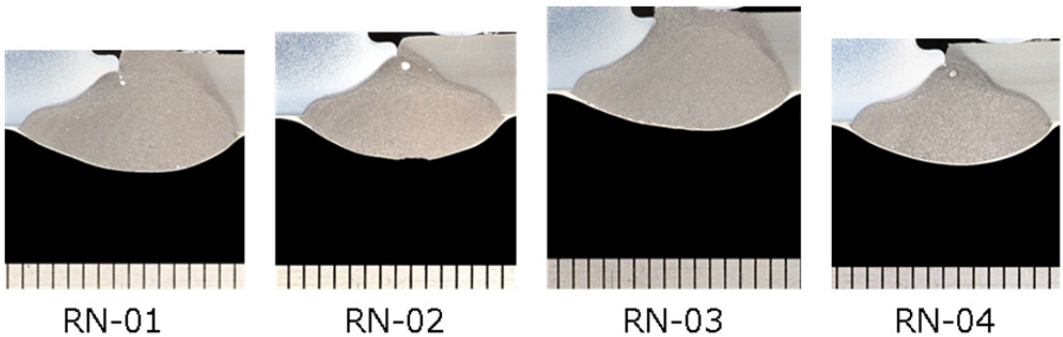


**Figure 15** Images of the circumferential welds from the rear nearside section of AT11-1475. Tick marks indicate 1.0mm length scale. The locations are shown in Figure 13.

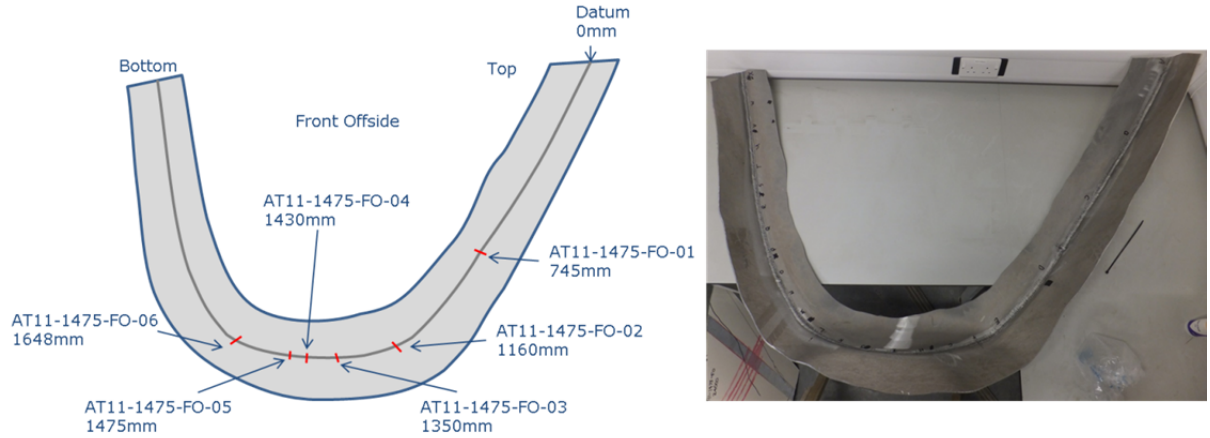


**Figure 16** Diagram of the sampling plan for the front offside (impacted) section of AT11-1475.

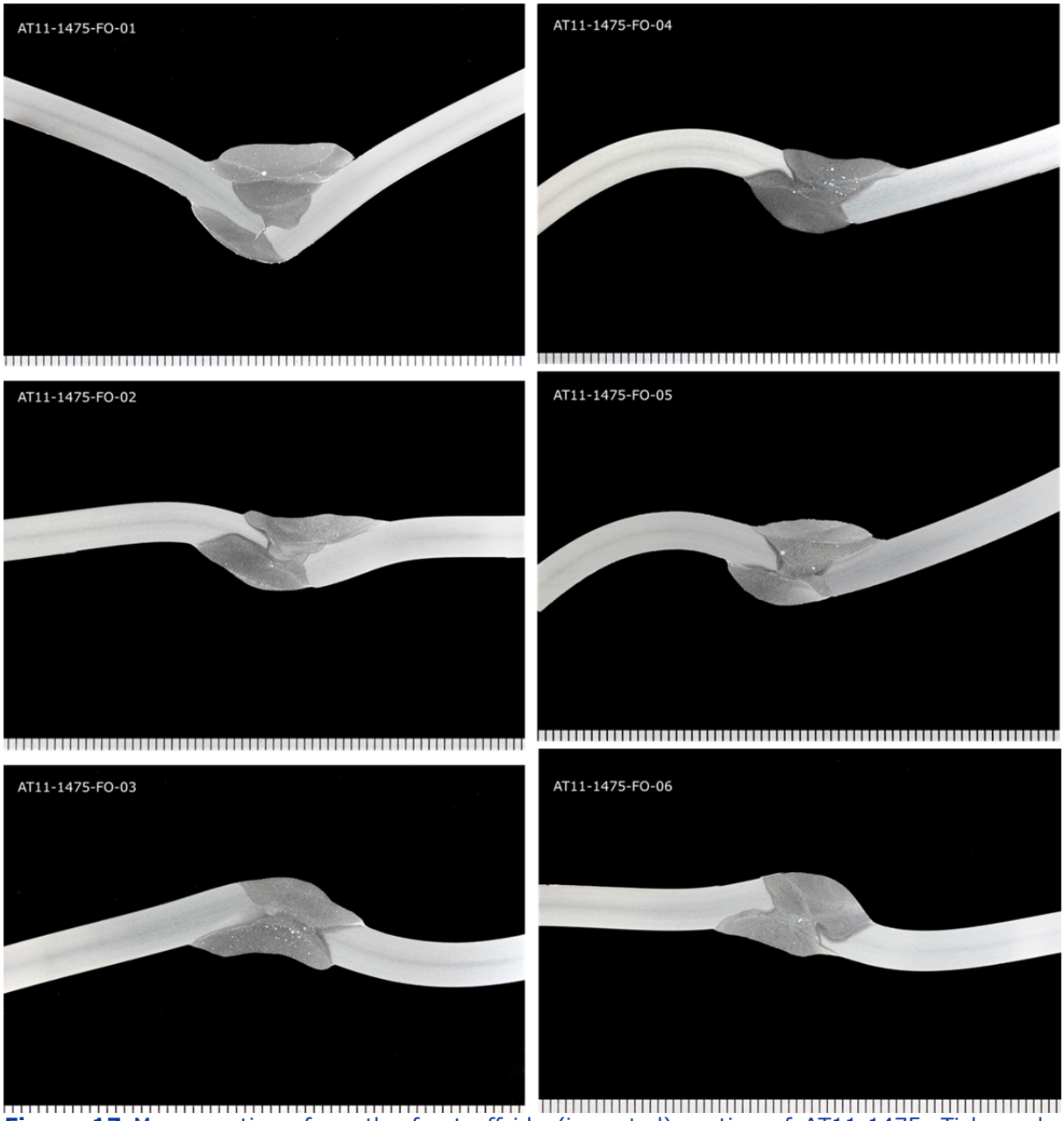


**Figure 17** Macro-sections from the front offside (impacted) section of AT11-1475. Tick marks indicate a 1.0mm length scale. The locations are shown in Figure 8.

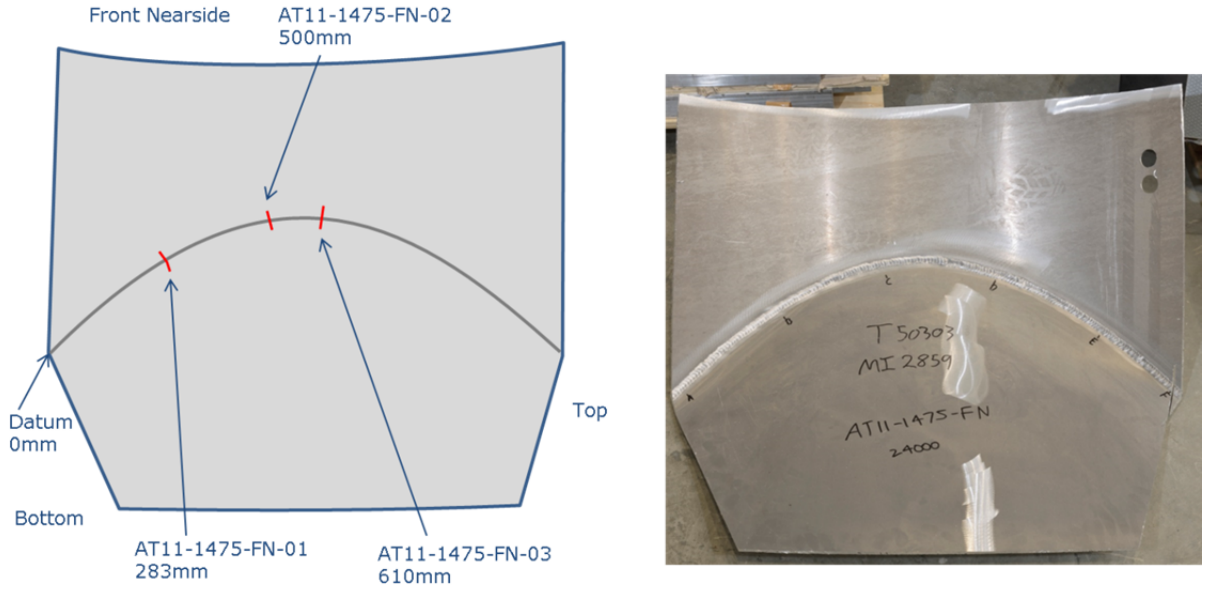


**Figure 18** Diagram of the sampling plan for the front nearside (undamaged) section of AT11-1475.

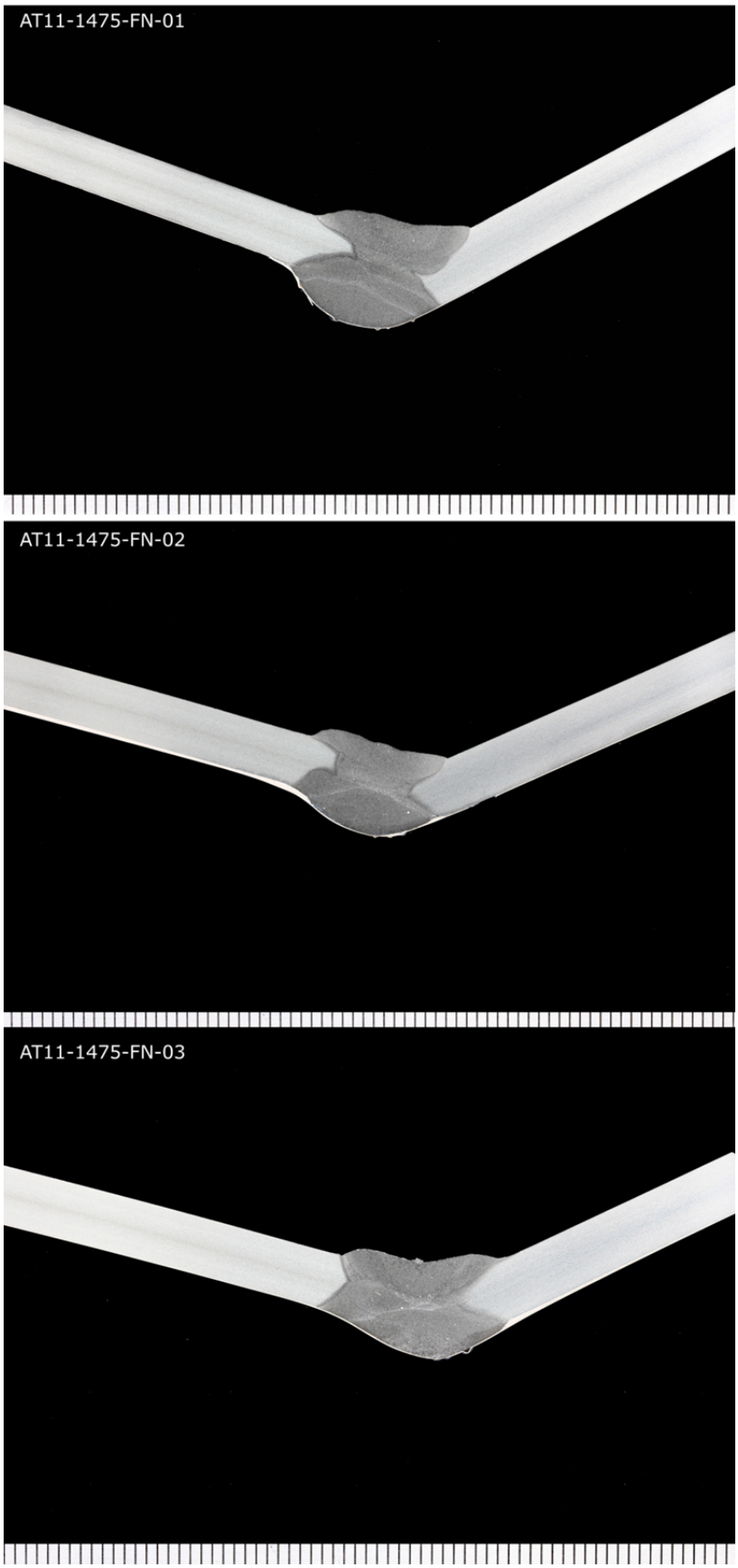


**Figure 19** Macro-sections from the front nearside (undamaged) section of AT11-1475. Tick marks indicate 1.0mm length scale. The locations are shown in Figure 10.

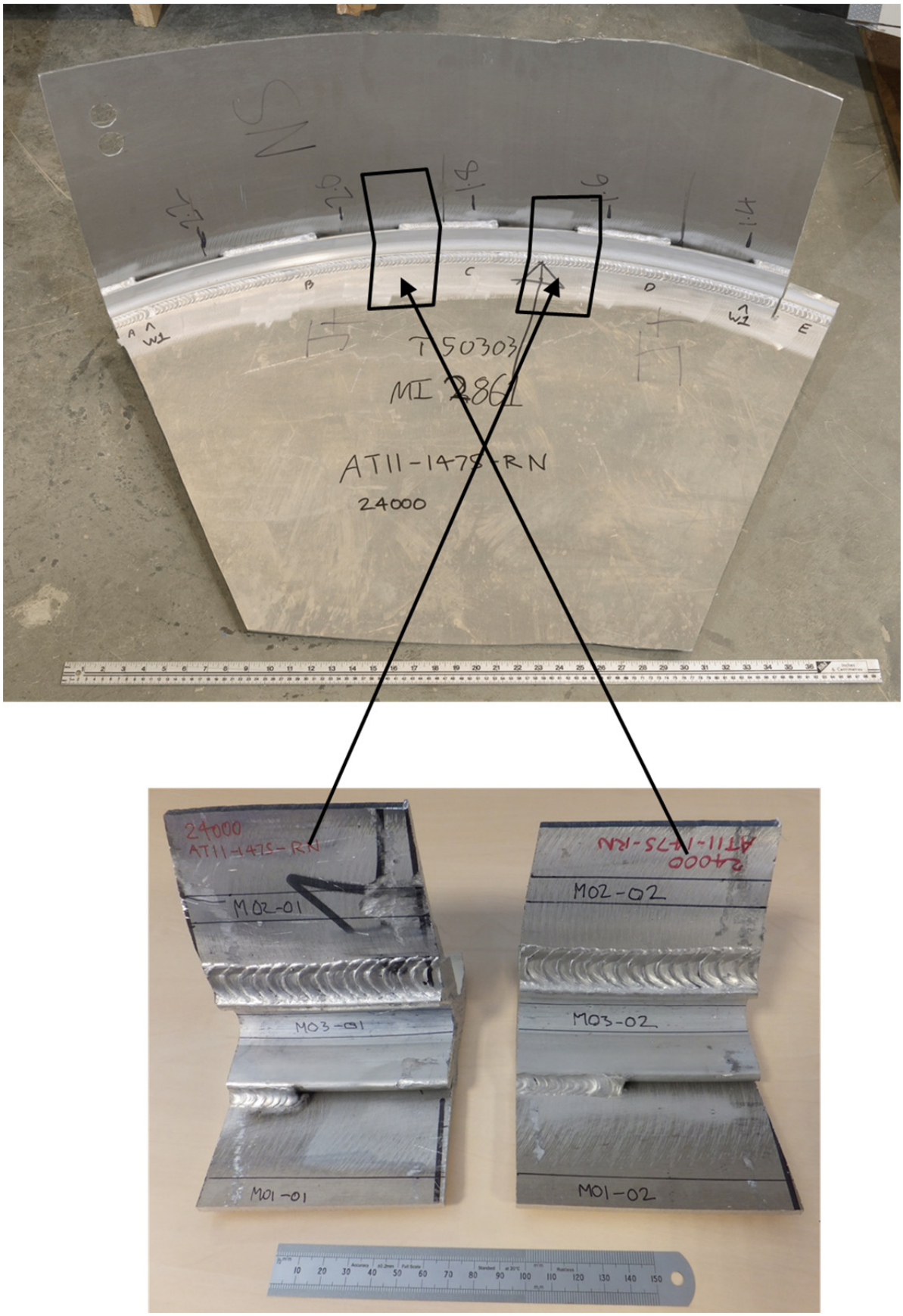


**Figure 20** Locations of the tensile specimens. The weld metal was taken from position E (top) as shown in Figure 1.

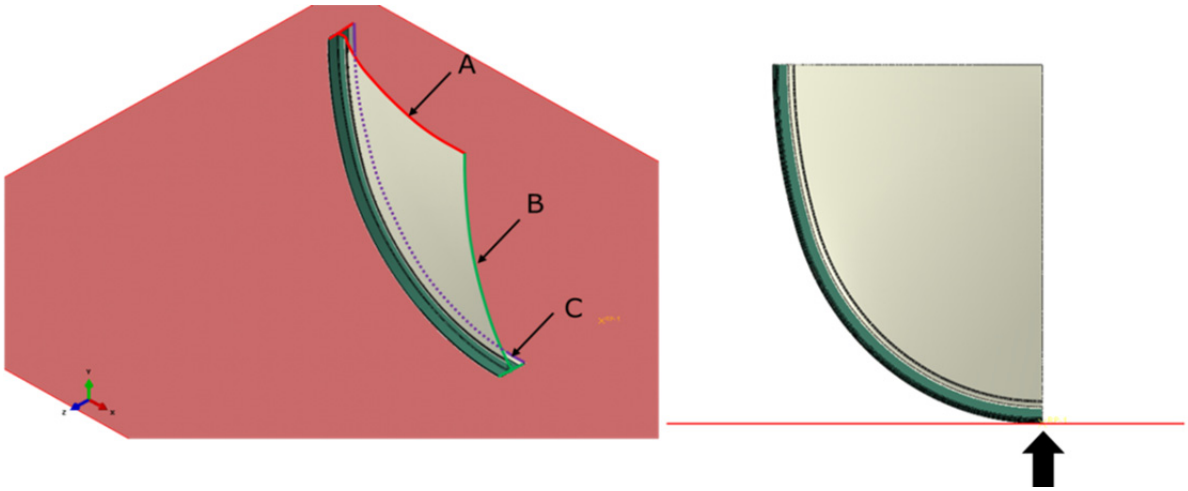


**Figure 21** Diagrams of the quarter-symmetry geometry of the finite element model for the rear dish, side impact model. A) Y-direction restraint; B) X-direction restraint, C) Z-direction restraint. The movement of the ground is shown by the black arrow. The beige colour corresponds to parent and weld metal and the green corresponds to the extrusion band metal.

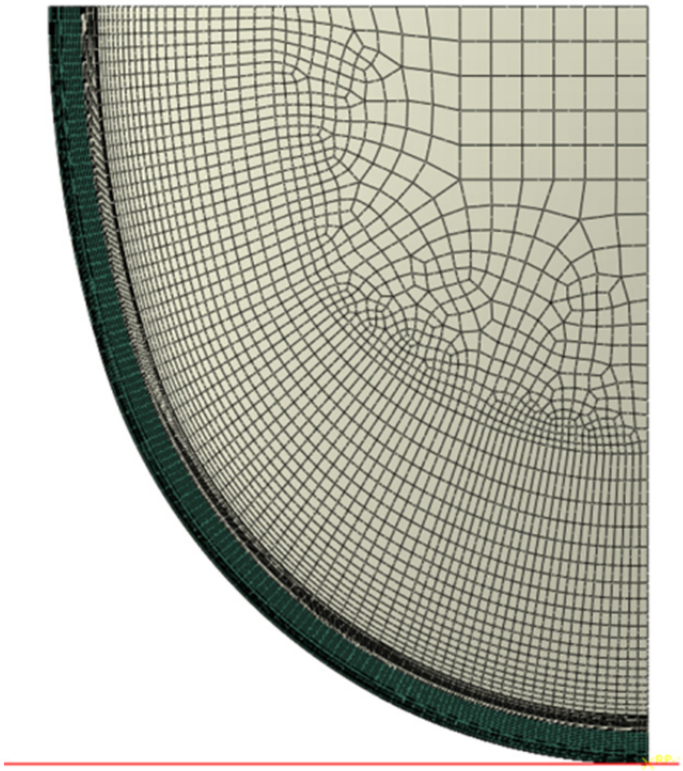

**Figure 22** Finite element mesh used for the rear dish, side impact model. The beige colour corresponds to parent and weld metal and the green corresponds to the extrusion band metal. Viewed from the front.

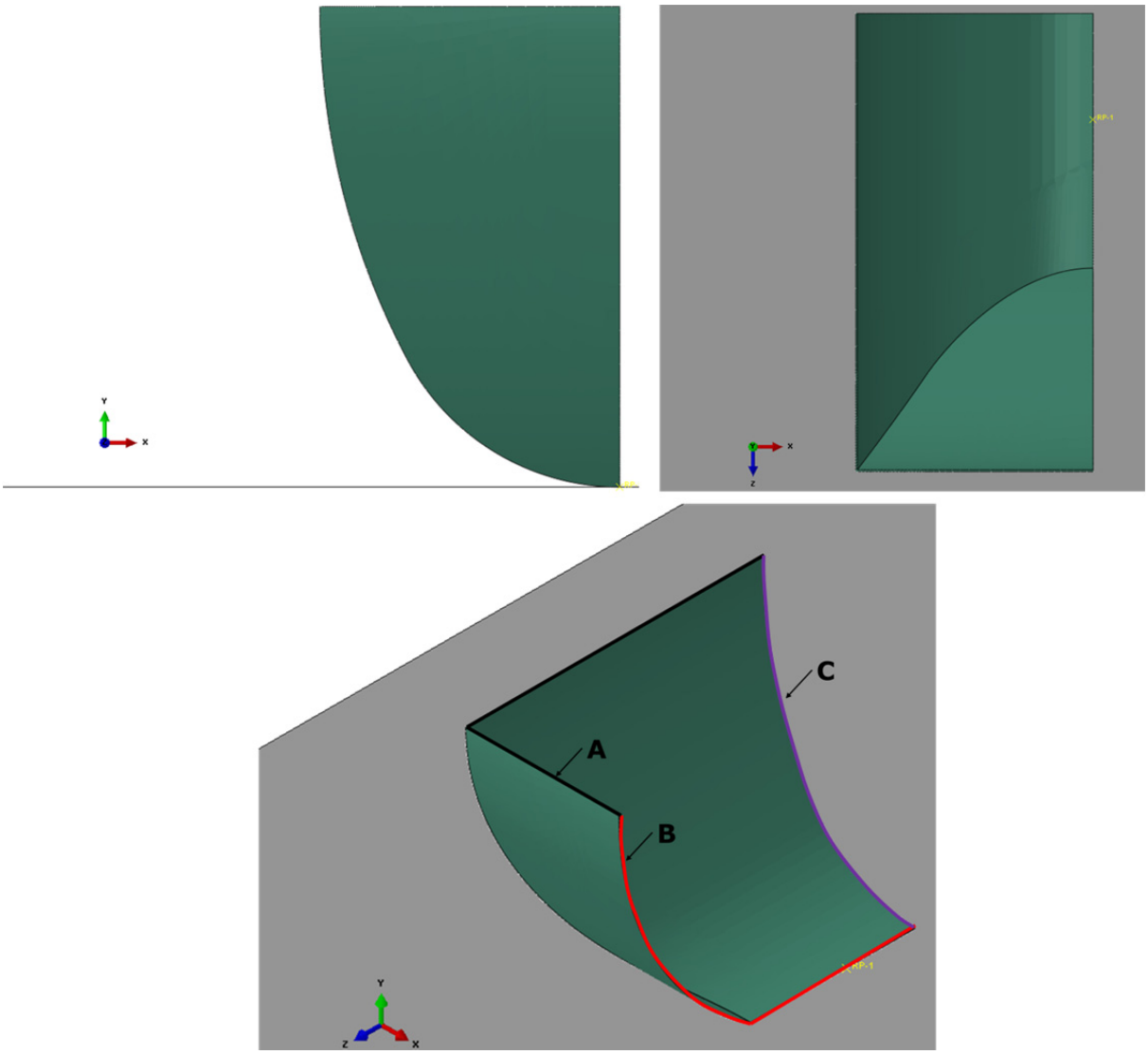


**Figure 23** Diagrams of the quarter-symmetry geometry of the finite element model for the front end, side impact model. A) Y-direction restraint; B) X-direction restraint; C) Z-direction restraint. The top right frame shows the profile of the swept end front dish designed as viewed from the 3 o'clock position looking towards the 9 o'clock position of the tank with upright.

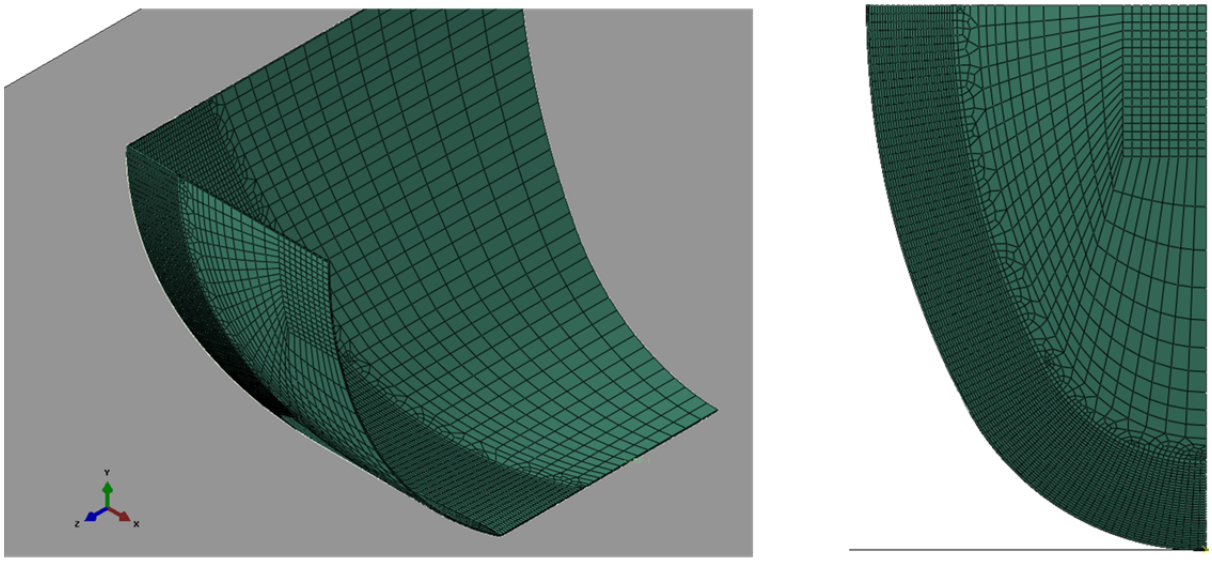

**Figure 24** Finite element mesh used for the front dish, side impact model.

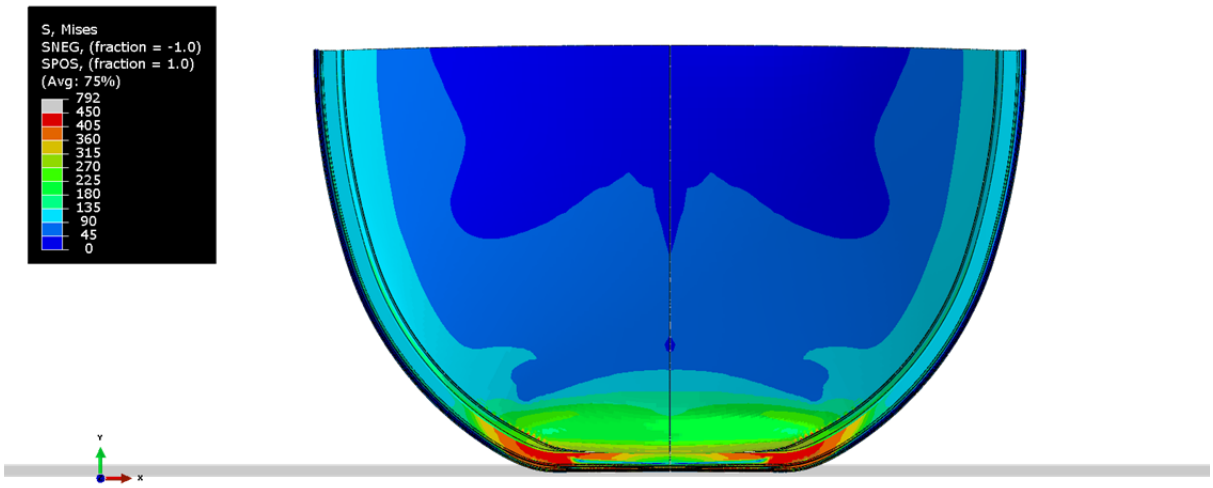


**Figure 25** Image of the rear dish (viewed from the back of the tanker) when the flattened length is approximately 760mm. The symmetric half of the quarter model has been added for visualisation purposes.

**Figure 26** FEA results superimposed on the macro-section AT11-1475-RO-05 taken from the centre of the crush zone (equivalent to the symmetry plane in the FE model). Deformation not magnified, and equivalent plastic strain contour shown for reference.

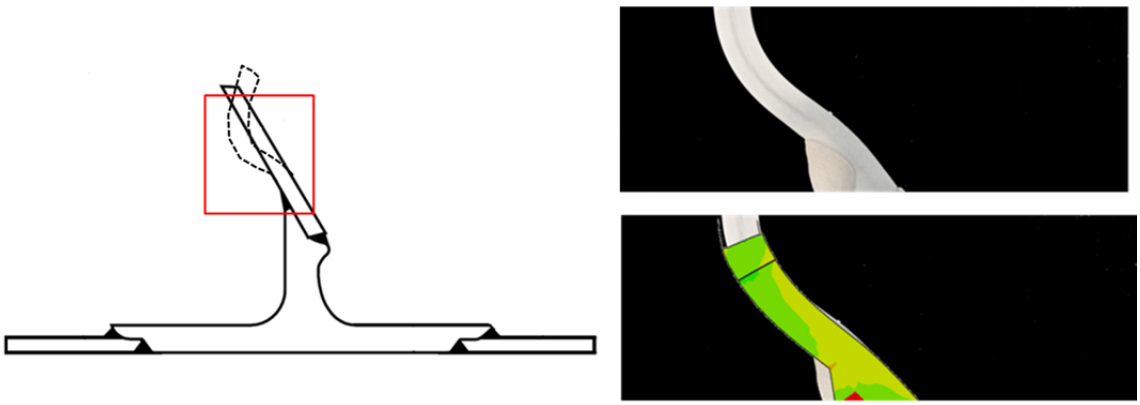

**Figure 27** FEA results superimposed on the macro-section AT11-1475-RO-03 taken from the end of the crush zone approximately 400mm from the centre of the crush zone.

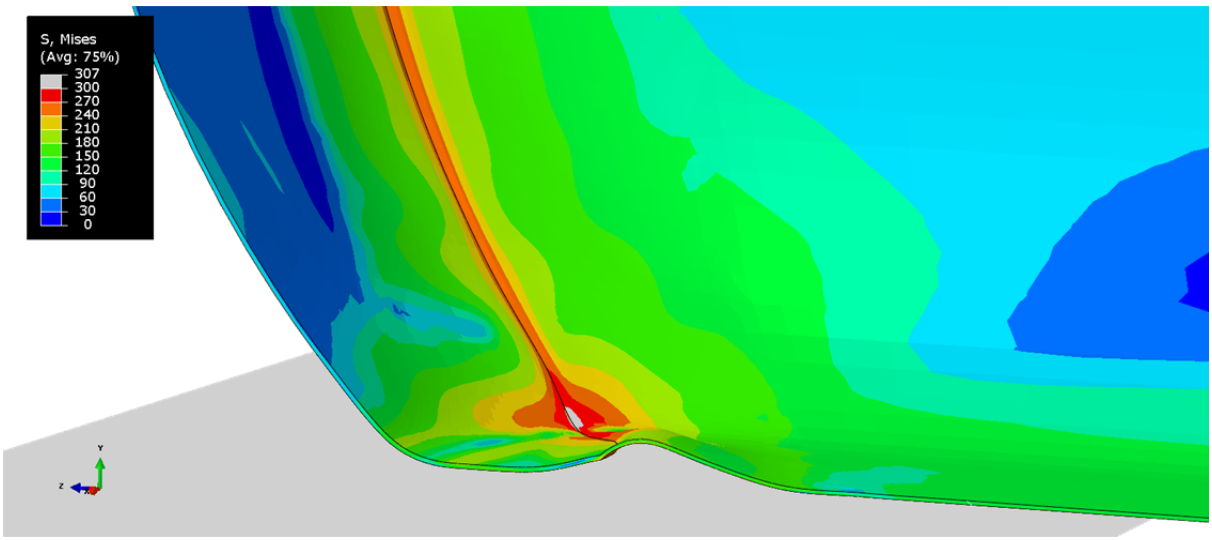


**Figure 28** Image of the front dish viewed along the central symmetry plane (ie the plane cutting the tank from 3 o'clock to 9 o'clock when upright) showing the deformation at the centre of the crush zone (see the right frames of Figure 17 for similar bending deformation).

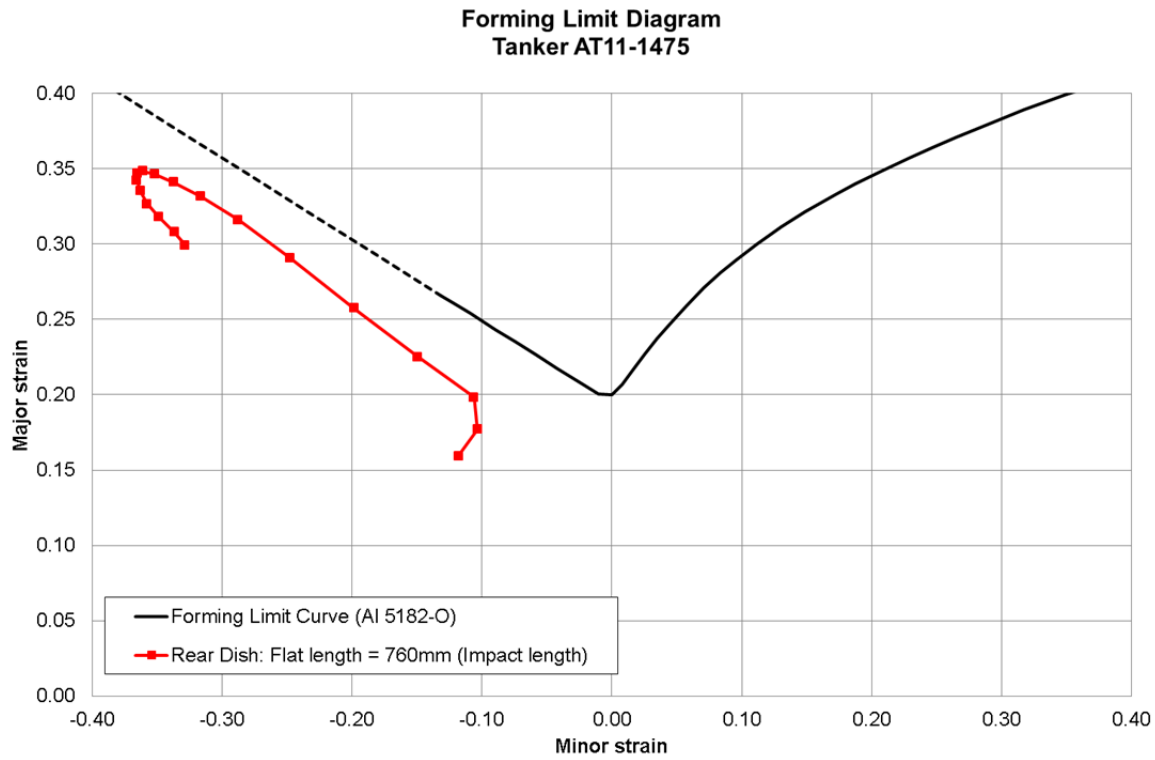


**Figure 29** Forming limit diagram for the rear dish simulation. Each red point represents the minor and major strains output at a node in the circumferential path passing through the most severely strained region of the model.

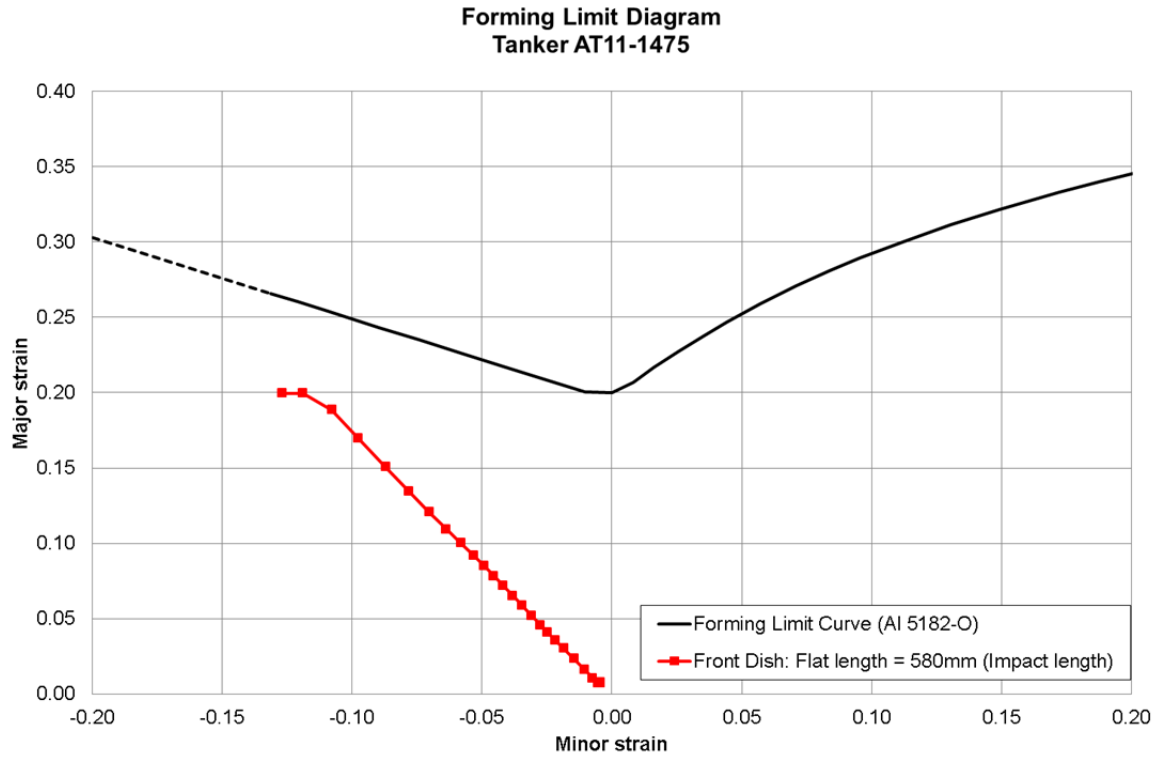


**Figure 30** Forming limit diagram for the front dish simulation. Each red point represents the minor and major strains output at a node in the circumferential path passing through the most severely strained region of the model.

**TWI Management System**

TWI operates a Management System designed to ensure that customer requirements are met and that any work carried out is conducted in a planned and controlled manner. Customer satisfaction is a key measure of the success of TWI, which remains committed to delivering world-class solutions. To this end:

- All technical activities are controlled by a management system that complies with the general requirements of the BS EN ISO 9000:2008 series of standards.

- Project management, examination and training services are audited by LRQA as complying with BS EN ISO 9001:2008 and software development in accordance with TickITplus, Certification Number 0925004.

- TWI is a UKAS accredited testing laboratory No. 0088. Specific details are given on the UKAS Schedule of Accreditation, available at www.ukas.org. Reports may contain information not included in the TWI schedule of accredited tests. Enquiries concerning accreditation of tests should be directed to the Quality and Safety Group.

- Examination activities are assessed by PCN to BINDT requirements and by TWI Certification Ltd to CSWIP requirements.

- TWI is certificated by LRQA to BS EN ISO 14001:2004, certificate number LRQA 4000756.

- TWI's Occupational Health and Safety Management System is certificated to BS OHSAS 18001:2007 by LRQA, certificate number 4004571.

The Management System operated by TWI includes the following features that are particularly relevant to ensuring the success of projects:

- Close and frequent contact with the customer is requested of the Project Leader throughout the project. In particular, changes in personnel involved in the project or equipment availability are discussed together with any project delays or contractual changes.

- Regular management reviews of projects are held throughout the life of a project and upon its completion. These cover finance, technical progress and adherence to schedule.

- Project sponsors are formally contacted on project completion by senior TWI management to determine their satisfaction with the work carried out. Moreover, TWI management welcomes feedback on project progress at all times during the course of the work. Significant lapses in service are subjected to a structured management review so that inadequate procedures are identified and improved.

TWI Ltd
Granta Park, Great Abington
Cambridge CB21 6AL
United Kingdom

Tel: +44 (0)1223 899000
Fax: +44 (0)1223 892588
Web: www.twi-global.com

VAT Number GB 700 1708 89

Registered Number 3859442 England